



Mechanochemical-Assisted Synthesis of Nitrogen-Doped Carbon Supported Cobalt Catalysts for Efficient and Selective Hydrogenation of Furfural

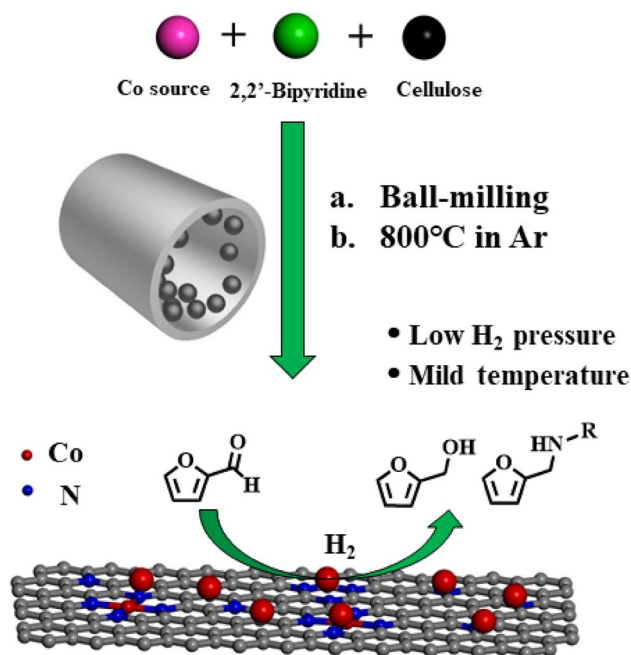
Song Han¹ · Wen-Ting Chen¹ · Zi-Teng Gao¹ · Hua Guan¹ · Zhang-Min Li¹ · Duan-Jian Tao¹

Received: 8 March 2022 / Accepted: 1 May 2022 / Published online: 19 May 2022
© The Author(s), under exclusive licence to Springer Science+Business Media, LLC, part of Springer Nature 2022

Abstract

A mechanochemical treatment and subsequent high temperature annealing strategy was developed for the synthesis of nitrogen-doped carbon supported cobalt catalysts. The as-prepared Co/NC₈₀₀ catalyst was demonstrated for efficient and selective hydrogenation of furfural into furfuryl-based alcohols and amines with good to excellent yields under optimum conditions.

Graphical Abstract



Graphical abstract

Keywords Furfural · Hydrogenation · Reductive amination · Cobalt catalyst · Nitrogen-doped carbon

✉ Zhang-Min Li
zml@jxnu.edu.cn

✉ Duan-Jian Tao
djtao@jxnu.edu.cn

Extended author information available on the last page of the article

1 Introduction

Efficient utilization of abundance and renewable biomass resources can slow down the usage amount of non-renewable fossil resources [1]. Natural biomass can be catalytically depolymerized to produce small molecular monomers such as furfural, 5-hydroxymethylfurfural, alcohols, organic acids, and esters [2–5]. As a typical biomass platform molecule, furfural is a dehydration product of xylose derived from hemicellulose [6]. It can be transformed to furfuryl-based alcohols [7, 8], furfuryl-based amines [9], and other high value-added chemical products by various catalytic processes such as hydrogenation, oxidation, and amination [10–12].

Up to now, many efficient methodologies have been studied for the preparation of furfuryl alcohol and furfuryl amine using furfural as raw material. For example, Long et al. prepared a noble metal nanoreactor Pt/CeO₂@MOF to achieve selective catalytic hydrogenation of furfural to furfuryl alcohol at 10 bar H₂ and 30 h [13]. After that, Qi and his co-workers reported a mesoporous carbon catalyst Ni@OMC for hydrogenation of furfural to furfuryl alcohol at 180 °C under a very high H₂ pressure of 30 bar [14]. Meanwhile, Iborra and his co-workers had studied the one-pot direct reductive amination of 5-hydroxymethylfurfural with aniline using Pd/C as a catalyst, yielding a series of *N*-substituted-5-(hydroxymethyl)-2-furfuryl amines [15]. Jiang et al. had used the Pd/Al₂O₃ catalyst to achieve the reduction of furfural to tetrahydrofuran-based secondary amines [16]. However, these progresses have suffered from several drawbacks such as using noble metal catalysts, low hydrogenation selectivity, and harsh reaction conditions (e.g. ~180 °C, ~20 bar H₂). Thus, increasing attention has been paid to the design and development of non-noble metal catalysts for efficient preparation of furfuryl-based alcohols and secondary amines under mild conditions [17, 18].

As well known, metal–support interaction is a significant impact factor of catalytic activity of supported metal catalyst systems. It can effectively affect the electronic properties, geometric morphologies, and/or chemical compositions of metal nanoparticles [19]. Nitrogen-doped mesoporous carbon has a large specific surface area and abundant mesopore, which has been widely used in the fields of heterogeneous catalysis and gas adsorption [20, 21]. For example, cobalt nanoparticles with good dispersion stability and uniform size distribution could be obtained through metal–support interaction between metallic cobalt and nitrogen-doped carbon material, which results in considerable hydrogenation reactivity [22, 23]. Furthermore, many studies have pointed out that a mechanochemical-assisted synthesis conducted by grinding

solid precursors together with no solvent shows greater efficiency for the preparation of nitrogen-doped carbon supported metal nanoparticles and outperforms the conventional solvent-based methods [24]. This mechanochemical-assisted synthesis strategy can avoid using the high toxicity of organic solvents and the additional cost for both the solvents and liquid wastes.

Herein, the nitrogen-doped carbon supported cobalt catalysts were prepared through a mechanochemical treatment and subsequent high temperature annealing, in which the Co/NC₈₀₀ catalyst exhibits good catalytic behavior in the selective reduction of furfural into furfuryl-based alcohols and amines using H₂ as hydrogen source under mild conditions. Systematic characterizations demonstrated that the Co/NC₈₀₀ catalyst showed the features of moderate mesoporosity, uniform Co nanoparticles, and metal–support interaction. In addition, the applicability of Co/NC₈₀₀ for selective hydrogenation of various aldehydes and ketones was further studied, and the catalytic reusability of Co/NC₈₀₀ was also investigated.

2 Experimental Section

2.1 Materials

Furfural (99%), tetrahydrofuran (THF, 99%), cobalt (II) acetate tetrahydrate [Co(Ac)₂·4H₂O, 99%], cobalt carbonate (CoCO₃, 98%), cobalt (II) acetylacetonate [Co(acac)₂, 97%], cobalt (II) nitrate hexahydrate [Co(NO₃)₂·6H₂O, 99%], and 2,2′-bipyridine (99%) were purchased from Shanghai Titan Scientific Co. Ltd. α-Cellulose (250 μm) was bought from Shanghai Aladdin Co. Ltd. All the chemicals were used as purchased without further treatment.

2.2 Synthesis of Co/NC_T Catalyst

Typically, 2,2′-bipyridine (6 mmol, 0.95 g) and α-cellulose (4 g) were added into a pot (50 mL) in a planetary ball milling instrument (YXQM-1L, MITR). Then a high-energy ball-milling procedure was carried out under 300 rpm for 1 h. Next, Co(NO₃)₂·6H₂O (2.5 mmol, 0.74 g) was put into the mixture and another ball-milling procedure was performed under 300 rpm for 2 h [25]. The obtained powder was thermally treated in a tubular furnace at a heating rate of 5 °C/min in a stream of argon at 800 °C for 2 h. After it had cooled to room temperature, a black powder was obtained and named Co/NC₈₀₀. Co/NC₇₀₀ and Co/NC₉₀₀ samples were obtained according to the above method, in which the pyrolysis temperature was set as 700 °C and 900 °C, respectively. For comparison, the NC₈₀₀ sample was synthesized in the same way with Co/NC₈₀₀ only without Co(NO₃)₂·6H₂O. Co/

NC_{800-ox} was obtained by treating Co/NC₈₀₀ at 250 °C for 1 h in air. Co/NC_{800-re} was acquired through a treatment of Co/NC₈₀₀ at 550 °C for 1 h in the mixed gas (10% H₂/90% N₂, v/v). In addition, the Co/C₈₀₀ sample was prepared by calcination at 800 °C for 1 h in the mixed gas (10% H₂/90% N₂, v/v) after activated carbon impregnated Co(NO₃)₂·6H₂O.

2.3 Catalyst Characterization

XRD patterns of samples were obtained on a Rigaku RINT-2200 X-ray diffractometer. The surface area and pore size distribution of the catalysts were recorded using a nitrogen adsorption/desorption analysis (Micromeritics Tristar 3020). The morphology and sizes of the catalysts were characterized by transmission electron microscopy (TEM, JEOL JEM-2100). The surface elemental composition of the sample was examined on AXIS Supra X-ray photoelectron spectroscopy (XPS, Kratos Analytical). The reduction performance of catalysts was analyzed by temperature-programmed reduction (H₂-TPR, Micromeritics Autochem II 2920).

2.4 Hydrogenation Process

In a typical run for selective hydrogenation reduction of furfural to furfuryl alcohol, 0.50 mmol furfural, 50.0 mg catalyst, and 5.0 mL THF were put into a 25 mL stainless steel autoclave. After three purging of the reactor with pure H₂, the reactor was then pressurized with H₂ and heated to 100 °C for 6.0 h with stirring at 600 rpm. Likewise, the one-pot reductive amination of furfural was carried out in a 25 mL stainless steel autoclave, followed by the introduction of 0.50 mmol furfural, 1.0 mmol aniline, 50.0 mg catalyst, and 5.0 mL THF. The reactor was further purged with H₂ three times and treated at 110 °C with stirring of 600 rpm.

After the reaction, the autoclave reactor was cooled down to 30 °C. The used catalyst was firstly separated from the reaction mixture through filtration. The recycled catalyst was washed with ethanol five times and reused after drying. The liquid products were qualitatively identified through gas chromatography-mass spectrometry (GC-MS, Thermo Trace 1300 GC-ISQ) and quantitatively analyzed using internal standard dodecane by gas chromatography (Thermo Trace 1310) with flame ionization detector.

3 Results and Discussion

3.1 Characterization of Co/NC_T Samples

Figure 1 shows the XRD patterns of Co/NC₇₀₀, Co/NC₈₀₀, and Co/NC₉₀₀ samples. It is found that a broad peak at 25° was ascribed to the (002) crystal plane of graphite-like

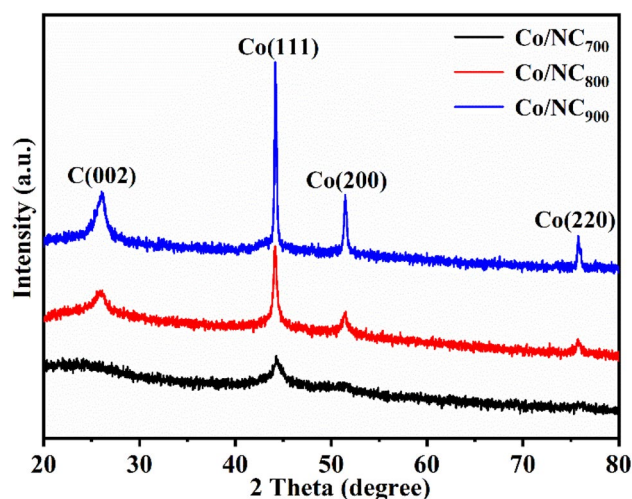


Fig. 1 XRD patterns of Co/NC₇₀₀, Co/NC₈₀₀, and Co/NC₉₀₀

carbon (PDF#41-1487). Also, the peaks located at $2\theta = 44.2^\circ$, 51.5° , and 75.9° were indexed to the Co (111), Co (200), and Co (220) crystalline planes of metallic Co⁰ phase (PDF#15-0806), respectively, indicating that metallic Co⁰ was formed after pyrolysis. Moreover, as the pyrolysis temperature raises from 700 °C to 900 °C, the peak intensity of metallic Co⁰ was strengthened gradually. According to Scheller's formula, the average Co crystallite sizes of these three samples were calculated to 16.6 nm, 17.1 nm, and 53.3 nm, respectively [14]. This implies that the agglomeration of Co particles would have occurred with the temperature increase in 900 °C. For comparison, Fig S1 and Table S1 show the XRD patterns and elemental analysis of the reference samples Co/NC_{800-ox} and Co/NC_{800-re}, respectively. It is indicated that the metallic Co⁰ phase was disappeared after calcination in air. The Co loading amount in Co/NC_{800-ox} was changed slightly, and Co₃O₄ crystals were generated in the Co/NC_{800-ox} sample. Besides, with a further reduction of Co/NC₈₀₀ using H₂ at 550 °C, the crystallinity of metallic Co⁰ phase in Co/NC_{800-re} was higher than that of Co/NC₈₀₀. This implies that the Co/NC_{800-re} sample would have a larger Co particle size.

The morphology and particle size distribution of Co/NC_T samples were characterized by TEM. As shown in Fig. 2a, Co/NC₈₀₀ sample presented the type of lamellar nanostructure and had a uniform distribution size of Co particles. The Co particles with an average size of 16.5 nm were well-dispersed on the support graphite-like carbon. The cobalt crystal plane spacing was also measured as 0.205 nm (Fig. 2a), which belongs to the (111) crystal plane of metallic Co⁰ (PDF#15-0806). For comparison, the TEM image illustrates that the Co nanoparticle in the Co/NC₇₀₀ was not uniform in size (Fig. 2b). The Co nanoparticles in Co/NC₉₀₀ and Co/C₈₀₀ samples were seriously aggregated to larger

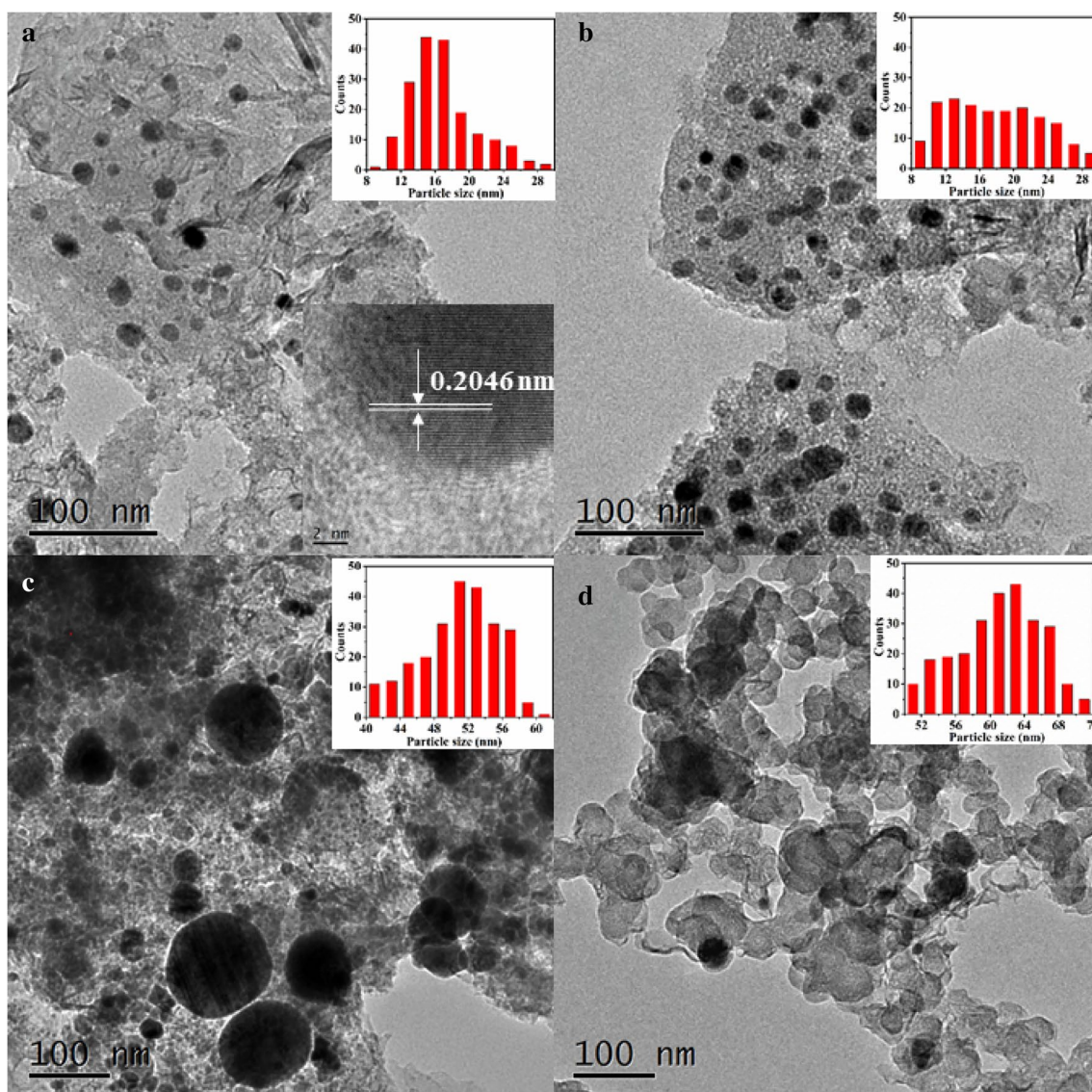


Fig. 2 **a** TEM (inset: Co nanoparticle size distribution and HRTEM) images of Co/NC₈₀₀; **b–d** TEM images of Co/NC₇₀₀, Co/NC₉₀₀ and Co/C₈₀₀ (inset: Co nanoparticle size distribution)

clusters (Fig. 2c, d). That means the *N*-containing precursor 2,2'-bipyridine and pyrolysis temperature of 800 °C are the key factors in highly dispersing Co particles on the Co/NC₈₀₀ sample. In addition, it is found that the Co/NC_{800-re} sample had the larger Co particle size with nonuniform distribution due to the further reduction of Co/NC₈₀₀ (Fig S2, Supplementary Information).

Figure 3 shows the N₂ adsorption/desorption isotherms of Co/NC_T samples at −196 °C. According to the IUPAC definitions, these three Co/NC_T samples had H4 hysteresis loops with IV isotherms, indicating their predominantly mesoporous structure. Moreover, the specific surface areas of Co/NC₈₀₀ and Co/NC₇₀₀ were found to be higher than 350 m²/g, which is much larger than that of Co/NC₉₀₀.

This suggests that excessive annealing temperature would cause the collapse of mesoporous structure and subsequent agglomeration of Co nanoparticles. In addition, the pore width distributions of Co/NC_T samples were also shown in Fig S3 in the Supplementary Information. It is indicated that the average pore diameters of these three Co/NC_T samples were centered at around 3.8 nm, reconfirming their abundant mesoporous porosities.

The XPS characterization for Co/NC₇₀₀, Co/NC₈₀₀, and Co/NC₉₀₀ samples were further studied. The C, N, O, and Co elements were detected in the full-scan spectra of Co/NC₈₀₀ in Fig S4 in the Supplementary Information. Then the Co 2p_{3/2} XPS spectra of Co/NC_T were deconvoluted to four peaks at 778.8, 780.7, 782.6, and 786.3 eV, which

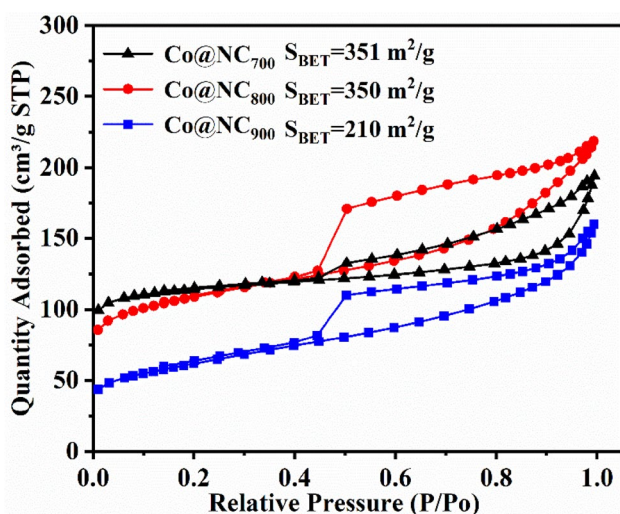


Fig. 3 N_2 adsorption–desorption isotherms of Co/NC_{700} , Co/NC_{800} , and Co/NC_{900} at $-196\text{ }^\circ\text{C}$

corresponds to metallic Co^0 , Co^{3+} , Co^{2+} , and Co^{2+} satellite, respectively (Fig. 4a). It is also found that increasing the pyrolysis temperature could enhance the percentages of Co^{3+} and Co^{2+} species but dramatically reduce the percentage of Co^0 species in Co/NC_T samples (Table S2, Supplementary Information). This suggests that most Co species would tend to form cobalt oxide at an over high annealing temperature. Moreover, Fig. 4b shows the N1s spectra of Co/NC_T samples. Three distinguishable peaks were found at 398.6, 401.0, and 402.2 eV, corresponding to pyridinic-N, pyrrolic-N, and graphitic-N, respectively.

The reducibility of Co/NC_T samples was performed by H_2 -TPR (Fig. 5). It is shown that a sharp intensive peak (centered at $359\text{ }^\circ\text{C}$) appeared in the H_2 -TPR profile, corresponding to the reduction of Co^{3+} to metallic Co^0 . [26] By contrast, there is no clear peak in the H_2 -TPR profile of $Co/$

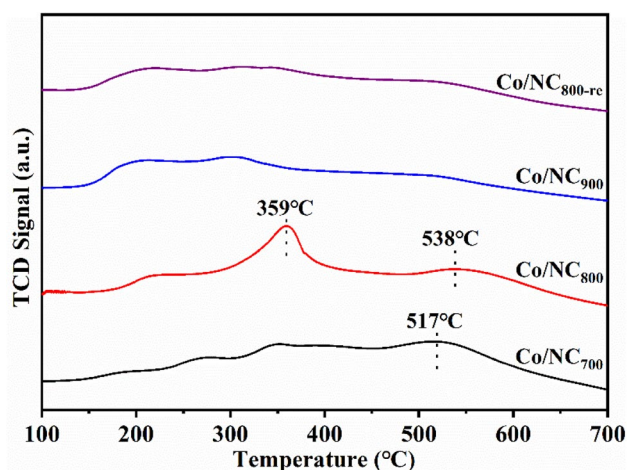


Fig. 5 H_2 -TPR of Co/NC_{700} , Co/NC_{800} , Co/NC_{900} and Co/NC_{800-re}

NC_{900} and Co/NC_{800-re} samples. This result reconfirms the uniform Co particles size and homogeneous morphology of Co/NC_{800} . [27] Moreover, a shoulder peak located at $538\text{ }^\circ\text{C}$ was further observed for Co/NC_{800} sample, indicating the presence of strong interaction between cobalt species and nitrogen-doped carbon support on the Co/NC_{800} sample [28].

3.2 Selective Hydrogenation of Furfural to Furfuryl Alcohol

Co/NC_T samples were employed as catalysts for selective catalytic hydrogenation furfural to furfuryl alcohol. The results are summarized in Table 1. Among the prepared Co/NC_T samples (Table 1, entries 1–3), the Co/NC_{800} catalyst exhibited the best catalytic performance in furfural hydrogenation, with a 99% conversion of furfural and over 99% selectivity of furfuryl alcohol. However, Co/NC_{700} and Co/NC_{900} only induced 60% and 48% conversions of furfural,

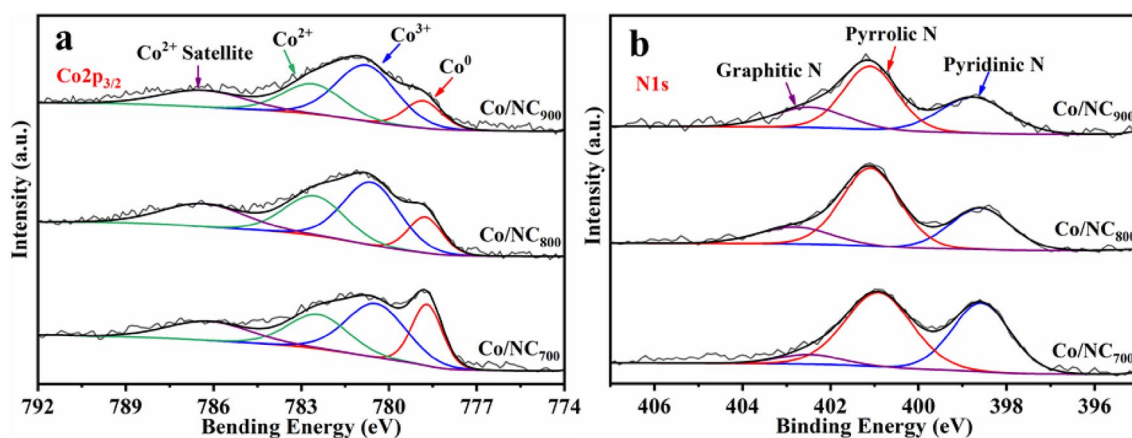
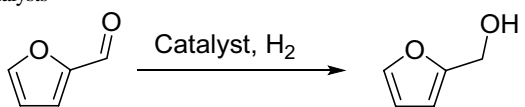


Fig. 4 XPS spectra of $Co\ 2p_{3/2}$ (a) and $N\ 1s$ (b) for Co/NC_{700} , Co/NC_{800} , and Co/NC_{900}

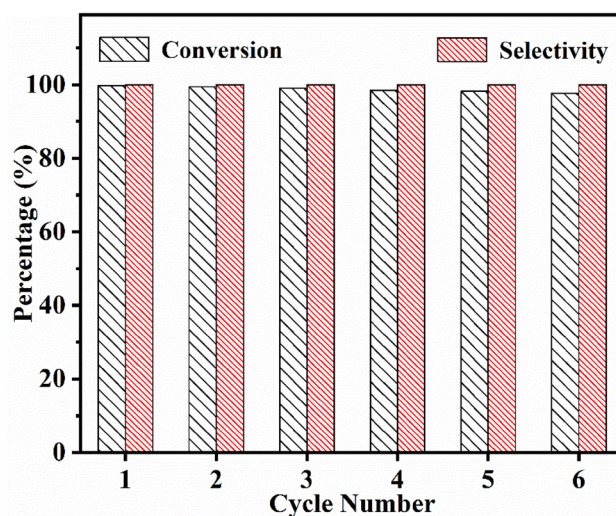
Table 1 Selective hydrogenation of furfural to furfuryl alcohol over different catalysts


Entry	Catalyst	Conversion (%)	Selectivity (%)
1	Co/NC ₇₀₀	60	> 99
2	Co/NC ₈₀₀	99	> 99
3	Co/NC ₉₀₀	48	> 99
4	Co/NC ₈₀₀₋₁	99	> 99
5	Co/NC ₈₀₀₋₂	99	> 99
6	Co/NC ₈₀₀₋₃	98	> 99
7	Co/C ₈₀₀	3	> 99
8	NC ₈₀₀	0	0
9	Co/NC _{800-ox}	3	> 99
10	Co/NC _{800-re}	63	> 99

Reaction condition: furfural (0.5 mmol), catalyst (50 mg), THF (5 mL), H₂ (6 bar), 600 rpm, 100 °C, 6 h. Co/NC₈₀₀₋₁, Co/NC₈₀₀₋₂, and Co/NC₈₀₀₋₃ was used Co(Ac)₂·4H₂O, Co(acac)₂ and Co(CO₃)₂ as cobalt resources, respectively. The products were analyzed by GC and GC-MS

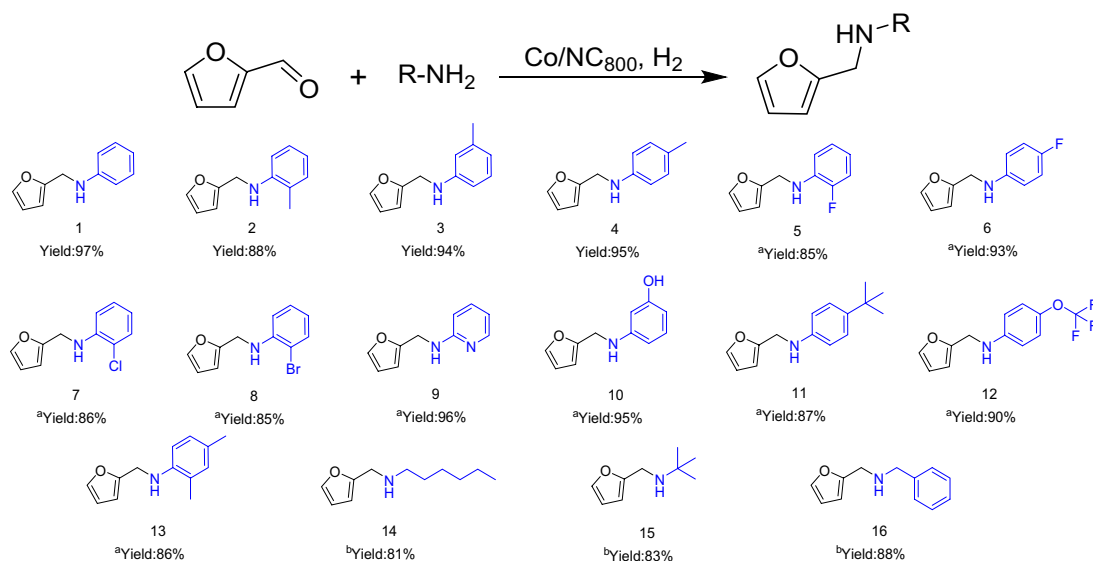
respectively. These results undoubtedly show that the features of relatively large surface area, moderate Co⁰ crystallinity, uniform size of Co nanoparticles, and metal–support interaction of cobalt species with nitrogen-doped carbon in the Co/NC₈₀₀ catalyst are responsible for the best catalytic activity for furfural hydrogenation. After screening the reaction conditions (Table 1, entries 1–3), the optimized conditions are as follows: 30 mol% Co/NC₈₀₀, THF as the solvent, 6 bar H₂, reaction temperature of 100 °C, and reaction time of 6 h (Figs S5–S7, Supplementary Information).

Moreover, various Co-based materials were further prepared and used as reference catalysts to clarify the excellent catalytic activity of Co/NC₈₀₀ in furfural hydrogenation (Table 1, entries 4–9). It is found that the Co/NC₈₀₀₋₁, Co/NC₈₀₀₋₂, and Co/NC₈₀₀₋₃ samples prepared by the other three cobalt salt precursors also exhibited good conversions of furfural and high selectivity of furfuryl alcohol (Table 1, entries 4–6). However, the Co/C₈₀₀ catalyst showed only 3% conversion of furfural under identical conditions (Table 1, entry 7) because of its serious aggregation of Co nanoparticles (Fig. 2d), demonstrating the importance of N-doping for the catalysis of Co/NC₈₀₀. The hydrogenation of furfural was not occurred using the sample NC₈₀₀ as catalyst (Table 1, entry 8), indicating that the cobalt nanoparticles would be the reactive species. Likewise, after treatment of extra oxidation, the Co/NC_{800-ox} sample with almost undetectable Co⁰ species (Fig. S8, Table S2, Supplementary Information)

**Fig. 6** Reusability test of Co/NC₈₀₀ in six runs

showed very poor activity for selective hydrogenation of furfural (Table 1, entry 9), verifying that Co⁰ species is the key catalytic active site. On the other hand, after a continuous reduction of Co/NC₈₀₀, the Co/NC_{800-re} catalyst had a relatively high crystallinity of metallic Co⁰ phase and possessed larger Co particle size with nonuniform distribution (Figs S1, S2, Supplementary Information), resulting in only 63% conversion of furfural (Table 1, entry 10). This demonstrates that the uniform size of Co particles is also beneficial to promote selective hydrogenation of furfural to furfuryl alcohol.

In addition, the comparison of the performance of Co/NC₈₀₀ with other catalysts systems in literature for selective catalytic hydrogenation of furfural to furfuryl alcohol was further listed in Table S3. It is demonstrated that for gaining considerable conversions of furfural, most of the previous catalysts systems were subject to harsh conditions such as high H₂ pressure and high temperature (e.g., 30 bar, 180 °C) [14, 29–33]. By contrast, while by using Co/NC₈₀₀ as the catalyst, hydrogen pressure could significantly reduce to 6 bar and a 99% yield of furfuryl alcohol was achieved under mild conditions. Finally, the recyclability and reusability of the Co/NC₈₀₀ catalyst were examined. As shown in Fig. 6, no obvious decline in furfural conversion and furfural alcohol yield was observed after 6 successive cycles, indicating good stability of Co/NC₈₀₀ under optimized reaction conditions. Compared to the fresh catalyst, the XRD patterns of the regenerated Co/NC₈₀₀ catalyst showed the well-preserved diffraction peaks of Co⁰ nanoparticles (Fig S9, Supplementary Information). This suggests that the Co/NC₈₀₀ catalyst is stable enough to be reused in selective hydrogenation of furfural to furfuryl alcohol.

Table 2 Reductive amination of furfural catalyzed by Co/NC₈₀₀

Reaction condition: furfural (0.5 mmol), amine (1 mmol), Co/NC_{800} (50 mg), THF (5 mL), H_2 (6 bar), 110 °C, 600 rpm, 6 h. The products were analyzed by GC–MS and GC–MS

^a120 °C

^b130 °C

3.3 Reductive Amination of Furfural to Furfuryl-based Amines

The preparation of furfuryl-based secondary amine through one-pot reductive amination of furfural was also studied and the results are presented in Table 2. The results show that a targeted product *N*-phenyl furfurylamine was obtained with a yield of 94% at 110 °C through the reaction of furfural with aniline catalyzed by the Co/NC_{800} catalyst (Table 2, entry 1). Also, the characterization results of ¹H NMR and ¹³C NMR confirmed the structure of *N*-phenyl furfurylamine (Fig S10, Supplementary Information). Moreover, various primary aromatic amines and aliphatic amines could be smoothly reacted with furfural to generate corresponding furfuryl-based secondary amines with 81–96% yields (Table 2, entries 2–16). All these products were confirmed by GC–MS (Fig S11, Supplementary Information). Notably, the reactivity of primary aliphatic amines was slightly weaker than that of primary aromatic amines. This is because that the π electron density of benzene ring in aromatic amine possess good conjugation with an amine group, which shows high reactivity for condensation of amine with furfural and subsequent formation of furfuryl-based secondary amine [34].

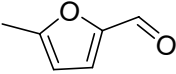
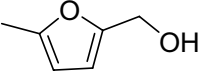
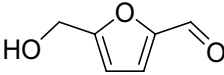
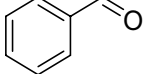
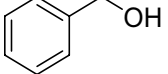
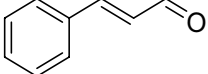
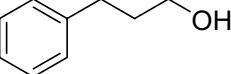
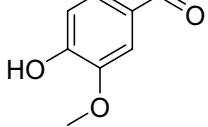
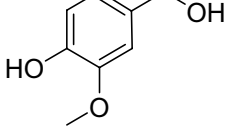
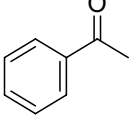
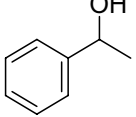
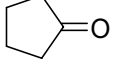
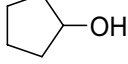
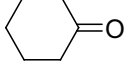
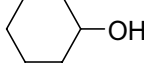
In addition, the comparison of the performance of Co/NC_{800} with other catalysts systems in literatures for the one-pot reductive amination of furfural was further listed in Table S4. It is shown that previous results relative to one-pot reductive amination of furfural relied on high hydrogen pressure (~20 bar) [35], high reaction temperature (~150 °C) or Pd

and Ru noble-metal catalysts [15, 36, 37]. By contrast, while by using Co/NC_{800} as a non-precious metal catalyst, hydrogen pressure could significantly reduce to 6 bar as well as reaction time decreased to 6 h, affording a 94% yield of *N*-phenyl furfurylamine. Therefore, Co/NC_{800} as a non-precious metal catalyst is demonstrated to be able to efficiently cleavage H_2 and hydroamination of furfural to *N*-phenyl furfurylamine, which results consequently in hydroamination process safety and cost-efficiency.

3.4 Selective Hydrogenation of Biomass-derived Aldehydes and Ketones

We further explored the catalysis of Co/NC_{800} in selective hydrogenation of various biomass-derived aldehydes and ketones. These results are summarized in Table 3. These alcohols products were determined and confirmed by GC–MS (Fig. S12, Supplementary Information). It is obvious that all kinds of aldehydes examined could be transformed to the corresponding alcohols with high yields of 82–98% (Table 3, entries 1–5). For example, 5-methylfurfural can be catalyzed to 5-methylfurfuryl alcohol with a 98% yield after 6 h. Moreover, the Co/NC_{800} catalyst also worked well for the hydrogenation of bioderived ketones to alcohols. Acetophenone, cyclopentanone, and cyclohexanone were successfully reduced to the corresponding alcohols with 89–100% yields (Table 3, entries 6–8). Therefore, Co/NC_{800} is also considered to be an outstanding hydrogenation catalyst for selective hydrogenation of various aldehydes and ketones under mild conditions.

Table 3 Selective hydrogenation of biomass-derived aldehydes and ketones catalyzed by Co/NC₈₀₀

Entry	Substrate	Product	Conversion (%)	Selectivity (%)
1			100	98
2 ^a			95	82
3 ^b			100	94
4 ^a			100	95
5 ^b			98	90
6 ^b			100	89
7 ^a			100	100
8 ^a			100	100

Reaction condition: substrate (0.5 mmol), Co/NC₈₀₀ (50 mg), THF (5 mL), H₂ (6 bar), 100 °C, 600 rpm, 6 h. The products were analyzed by GC and GC-MS

^a120 °C, 10 h

^b90 °C, 8 h

4 Conclusion

In this work, nitrogen-doped carbon supported cobalt catalysts were successfully prepared by a simple ball milling procedure and subsequent pyrolysis treatment. It is found that the as-prepared Co/NC₈₀₀ catalyst displayed outstanding catalytic activity and stability toward hydrogenation of furfural and one-pot reduction amination of furfural, respectively, affording the target products furfuryl-based alcohols and secondary amines with the yields of more than 80%. Moreover, the Co/NC₈₀₀ catalyst also catalyzed selective catalytic hydrogenation of biomass-derived aldehydes and ketones to obtain the corresponding product alcohols with 82% ~ 100% yields. The results of control experiments and several characterizations further

demonstrated that the features of abundant mesoporosity, high dispersity and uniform size distribution of Co nanoparticles, and metal-support interaction of cobalt species with nitrogen-doped carbon accounted for the best catalytic performance of the Co/NC₈₀₀ catalyst. It is considered that the utilization of non-noble cobalt-based catalysts is an effective strategy to directly transform furfural into high value-added furfuryl derivatives.

Supplementary Information The online version contains supplementary material available at <https://doi.org/10.1007/s10562-022-04042-y>.

Acknowledgements We gratefully thank the Key Research and Development Program of Jiangxi Province (Grant No. 20202BBGL73118) and the National Natural Science Foundations of China (Grant No. 22068013) for financial support.

Declarations

Conflict of interest The authors declare no competing financial interest.

References

1. Vispute TP, Zhang H, Sanna A, Xiao R, Huber GW (2010) *Science* 330:1222
2. Besson M, Gallezot P, Pinel C (2014) *Chem Rev* 114:1827–1870
3. Sun D, Sato S, Ueda W, Primo A, Garcia H, Corma A (2016) *Green Chem* 18:2579–2597
4. Wan X, Zhou C, Chen J, Deng W, Zhang Q, Yang Y, Wang Y (2014) *ACS Catal* 4:2175–2185
5. Siddiki SMAH, Touchy AS, Kon K, Toyao T, Shimizu K (2017) *ChemCatChem* 9:2816–2821
6. Zhang X, Wilson K, Lee AF (2016) *Chem Rev* 116:12328–12368
7. Guo H, Zhang H, Zhang L, Wang C, Peng F, Huang Q, Xiong L, Huang C, Ouyang X, Chen X, Qiu X (2018) *Ind Eng Chem Res* 57:498–511
8. Deng Y, Gao R, Lin L, Liu T, Wen X, Wang S, Ma D (2018) *J Am Chem Soc* 140:14481–14489
9. Galletti P, Montecavalli A, Moretti F, Pasteris A, Samorì C, Tagliavini E (2009) *New J Chem* 33:1859–1868
10. Li X, Jia P, Wang T (2016) *ACS Catal* 6:7621–7640
11. Nakagawa Y, Tamura M, Tomishige K (2013) *ACS Catal* 3:2655–2668
12. Seemala B, Cai CM, Wyman CE, Christopher P (2017) *ACS Catal* 7:4070–4082
13. Long Y, Song S, Li J, Wu L, Wang Q, Liu Y, Jin R, Zhang H (2018) *ACS Catal* 8:8506–8512
14. Tang Y, Qiu M, Yang J, Shen F, Wang X, Qi X (2021) *Green Chem* 23:1861–1870
15. García-Ortiz A, Vidal JD, Climent MJ, Concepción P, Corma A, Iborra S (2019) *ACS Sustain Chem Eng* 7:6243–6250
16. Jiang S, Muller E, Jérôme F, PeraTitus M, De Oliveira VK (2020) *Green Chem* 22:1832–1836
17. Chen S, Wojcieszak R, Dumeignil F, Marceau E, Royer S (2018) *Chem Rev* 118:11023–11117
18. Irrgang T, Kempe R (2020) *Chem Rev* 120:9583–9674
19. Gu J, Jian M, Huang L, Sun Z, Li A, Pan Y, Yang J, Wen W, Zhou W, Lin Y, Wang H, Liu X, Wang L, Shi X, Huang X, Cao L, Chen S, Zheng X, Pan H, Zhu J, Wei S, Li W, Lu J (2021) *Nat Nanotechnol* 16:1141–1149
20. Zhu Q, Li F, Zheng Y, Cao Y, Xiao Y, Liang S, Liu F, Jiang L (2022) *Purif Technol* 284:120272
21. Zheng W, Kan X, Liu F, Li H, Song F, Xia G, Liu J, Liu F (2022) *ACS Sustain Chem Eng* 10:3477–3487
22. Parastaev A, Muravev V, Huertas Osta E, van Hoof AJF, Kimpel TF, Kosinov N, Hensen EJM (2020) *Nat Catal* 3:526–533
23. Cheng Q, Liu Y, Lyu S, Tian Y, Ma Q, Li X (2021) *Chin J Chem Eng* 35:220–230
24. Qi H, Yang J, Liu F, Zhang L, Yang J, Liu X, Li L, Su Y, Liu Y, Hao R, Wang A, Zhang T (2021) *Nat Commun* 12:3295
25. Zhang P, Chen N, Chen D, Yang S, Liu X, Wang L, Wu P, Phillip N, Yang G, Dai S (2018) *ChemCatChem* 10:3299–3304
26. Zhou Y, Liu L, Li G, Hu C (2021) *ACS Catal* 11:7099–7113
27. Tang X, Zhang B, Li Y, Xu Y, Xin Q, Shen W (2004) *Catal Lett* 97:163–169
28. Ma L, Chen P, Zhang G, Wang L, Tang F, Zhao X, Wang J, Huang J, Liu Y (2021) Promoting H₂ activation over molybdenum carbide by modulation of metal–support interaction for efficient catalytic hydrogenation. *ChemCatChem* 13:3283–3289
29. Meng X, Yang Y, Chen L, Xu M, Zhang X, Wei M (2019) *ACS Catal* 9:4226–4235
30. Fan Y, Li S, Wang Y, Zhuang C, Liu X, Zhu G, Zou X (2020) *Nanoscale* 12:18296–18304
31. Fan Y, Zhuang C, Li S, Wang Y, Zou X, Liu X, Huang W, Zhu G (2021) *J Mater Chem A* 9:1110–1118
32. Yang Y, Chen L, Chen Y, Liu W, Feng H, Wang B, Zhang X, Wei M (2019) *Green Chem* 21:5352–5362
33. Gong W, Lin Y, Chen C, Al-Mamun M, Lu H, Wang G, Zhang H, Zhao H (2019) *Adv Mater* 31:1808341
34. Layer RW (1963) *Chem Rev* 63:489–510
35. Nuzhdin AL, Bukhtiyarova MV, Bukhtiyarova GA (2020) *J Chem Technol Biotechnol* 95:3292–3299
36. Chieffi G, Braun M, Esposito D (2015) *Chemsuschem* 8:3590–3594
37. Xu Z, Yan P, Xu W, Jia S, Xia Z, Chung B, Zhang ZC (2014) *RSC Adv* 4:59083–59087

Publisher's Note Springer Nature remains neutral with regard to jurisdictional claims in published maps and institutional affiliations.

Authors and Affiliations

Song Han¹ · Wen-Ting Chen¹ · Zi-Teng Gao¹ · Hua Guan¹ · Zhang-Min Li¹ · Duan-Jian Tao¹

¹ Key Laboratory of Functional Small Molecules for Ministry of Education, College of Chemistry and Chemical Engineering, Jiangxi Normal University, Nanchang 330022, Jiangxi, China